Hybrid Data Assimilation without Ensemble Filtering

Ricardo Todling* and Amal El Akkraoui†

Global Modeling and Assimilation Office, NASA/GSFC, Greenbelt, Maryland

* *Corresponding author address:* Dr. Ricardo Todling, Global Modeling and Assimilation Office, NASA/GSFC, Code 610.1, Greenbelt, MD 20771.

E-mail: ricardo.todling@nasa.gov

† *Additional Affiliation*: Science Systems and Applications, Inc., Lanham, MD 20706.

ABSTRACT

The Global Modeling and Assimilation Office is preparing to upgrade its three-dimensional variational system to a hybrid approach in which the ensemble is generated using a square-root ensemble Kalman filter (EnKF) and the variational problem is solved using the Grid-point Statistical Interpolation system. As in most EnKF applications, we found it necessary to employ a combination of multiplicative and additive inflations, to compensate for sampling and modeling errors, respectively and, to maintain the small-member ensemble solution close to the variational solution, we also found it necessary to re-center the members of the ensemble about the variational analysis. During tuning of the filter we have found re-centering and additive inflation to play a considerably larger role than expected, particularly in a dual-resolution context when the variational analysis is ran at larger resolution than the ensemble. This led us to consider a hybrid strategy in which the members of the ensemble are generated by simply converting the variational analysis to the resolution of the ensemble and applying additive inflation, thus bypassing the EnKF. Comparisons of this, so-called, filter-free hybrid procedure with an EnKF-based hybrid procedure and a control non-hybrid, traditional, scheme show both hybrid strategies to provide equality significant improvement over the control; more interestingly, the filter-free procedure was found to give qualitatively similar results to the EnKF-based procedure.

1. Introduction

It is now generally accepted that a practical feasible way to introduce flow dependence in the background error covariances needed for either sequential or variational data assimilation procedures is to rely on an ensemble of short-range forecasts. Multiple works have now shown (Whitaker et al. 2008, Buehner et al. 2010, and Clayton et al. 2012) that combining the time-varying background error covariance derived from an ensemble of forecasts with the typical, stationary, climatological background error covariance leads to non-trivial improvements to the resulting, so-called, hybrid data assimilation system (Lorenc 2003). Most operational weather centers use three- or four-dimensional variational (3D/4DVar) techniques and have implemented hybrid approaches in these contexts. With the variational component capable of accepting hybrid formulations of its underlying background error covariance, what remains to be specified is a methodology to generate the required ensemble of forecasts. Presently, the Global Modeling and Assimilation Office, follows the National Centers for Environmental Predictions, and uses the square-root-based ensemble Kalman filter (EnKF; Whitaker et al. 2008) for this purpose. The small number of ensemble members used in practice requires care to render adequate spread from the ensemble of forecasts to represent forecast errors. It is thus necessary to fiddle with the ensemble of analyses and: (i) apply multiplicative inflation to compensate for sampling errors; (ii) apply additive inflation to represent model uncertainties; and (iii) re-center the ensemble of analyses around the, hybrid, variational analysis to prevent possible divergence between the two assimilation systems.

During the process of implementation and testing of the EnKF to provide initial conditions for the ensemble of forecasts for a hybrid strategy to be adopted for the Goddard Earth

Observing System (GEOS) atmospheric data assimilation system (ADAS), we have found steps (ii) and (iii) above to play a significant role in determining the behavior of the ensemble of forecasts. This is particularly noticeable when the ensemble and the (hybrid) variational analyses are produced at different resolutions in a, so-called, dual resolution approach. That re-centering and additive inflation are such key components of the hybrid strategy is illustrated in Fig. 1, where the incremental contribution to the 500 hPa temperature field is shown for an arbitrarily selected member of the ensemble, at an arbitrarily selected time, after the EnKF has cycled beyond a spin up period. The panels in the figure correspond to increments at various stages in the ensemble analysis procedure: directly from the EnKF (top left), when only multiplicative inflation has been applied; when the EnKF increment is re-centered around the (hybrid) variational (higher resolution) analysis (top right); when applying additive inflation to the EnKF increment (bottom left); and when multiplicative inflation, additive inflation, and re-centering have been applied to form the total increment (bottom right). Re-centering is clearly a larger contributor to the total increment. Still, the main features in the increment obtained from the EnKF assimilation of observations are visibly identified after re-centering and additive inflation have taken place. At first, these results might suggest the EnKF to be poorly tuned, however, as we will show later, this is far from being the case. One key factor is that the EnKF analyses are at coarser resolution than the (hybrid) variational analysis used for re-centering; when the ensemble is at full resolution, the contribution from re-centering is much lesser (not shown).

The crucial role played by steps (ii) and (iii) prompted us to investigate what would happen if we bypassed the EnKF step altogether. This led us to the, so-called, filter-free ensemble scheme when ensemble analyses are generated by simply adding perturbations to the central, hybrid, variational analysis – that is, steps (ii) and (iii) are what constitute the ensemble analysis strategy. The additive perturbations used in this procedure correspond to samples of the scaled, 48-minus-24-hour forecast differences, similar to those used to generate the climatological background error covariance of the traditional assimilation approach; these are also the perturbations used when the EnKF is exercised. The remaining of this manuscript presents a comparison of results obtained from dual-resolution hybrid 3DVar procedures when either the EnKF or the filter-free approach is used for the ensemble analysis generation.

2. Brief overview and the filter-free strategy

The basic idea of hybrid variational data assimilation is to use an ensemble of background fields to introduce instantaneous, flow-dependent, features to the traditionally non-evolving (static) background error covariance. In 3DVar this can be done by augmenting the control vector with an extra set of variables, usually referred to as alpha-control variables. The cost function of a hybrid incremental 3DVar system can be written as

$$J(\delta\mathbf{z}) = \frac{1}{2}\delta\mathbf{z}^T \left[\beta_s\mathbf{B}_s + \beta_e\mathbf{T}^T(\mathbf{B}_e \circ \mathbf{L})\mathbf{T}\right]^{-1} \delta\mathbf{z} + \frac{1}{2}(\mathbf{d} - \mathbf{H}\delta\mathbf{z})^T\mathbf{R}^{-1}(\mathbf{d} - \mathbf{H}\delta\mathbf{z})\,, \qquad (1)$$

where the control variable $\delta\mathbf{z}$ is a combined contribution from the n-vector solution $\delta\mathbf{x}$ of the standard variational problem and a component that comes from an M-member ensemble, that is,

$$\delta\mathbf{z} = \beta_s\delta\mathbf{x} + \beta_e\mathbf{T}^T\sum_{m=1}^{M}\boldsymbol{\alpha}_m \circ \Delta\mathbf{w}^e_m\,. \qquad (2)$$

Here, the symbol $\circ$ stands for the Hadamard-Schur (element-wise) product of two vectors, $\boldsymbol{\alpha}_m$ is the m-th control vector related to the m-th ensemble member, and, using the symbol Δ to denote deviation from the mean, $\Delta\mathbf{w}_m^e = (\mathbf{w}_m^b - \bar{\mathbf{w}})/\sqrt{M-1}$ is the m-th ensemble perturbation created from the m-th member background n_w-vector state $\mathbf{w}_m^b$, with respect to the ensemble mean $\bar{\mathbf{w}}^b$. The formulation allows for the ensemble members to be of different (usually lower) resolution, than the primary n-vector control $\delta\mathbf{x}$, with the operator $\mathbf{T}^T$ being responsible for resolution conversion. In (1), the matrices $\mathbf{B}_s$ and $\mathbf{B}_e$ stand for the static and ensemble background error covariances, respectively; the matrix $\mathbf{L}$ stands for a correlation matrix responsible for localization of the ensemble; the last term is the usual observation-fit term involving the observation error covariance matrix $\mathbf{R}$, and the observation residual p-vector $\mathbf{d} = \mathbf{y} - \mathbf{h}(\mathbf{x}^g)$ created from differencing the observation p-vector $\mathbf{y}$ with the projection of the first-guess state-vector $\mathbf{x}^g$ onto observation space by the observation operator $\mathbf{h}$, whose linearization is represented by the matrix $\mathbf{H}$. The parameters β_s and β_e specify the interplay between the static and the ensemble background error covariances, respectively. The problem is reset to its traditional 3DVar configuration, with solution $\delta\mathbf{x}$, when $\beta_s = 1$ and $\beta_e = 0$. Details of the hybrid variational problem can be found in Hamill and Snyder (2000), Lorenc (2003) and Wang et al. (2007).

The *first* hybrid implementation studied in the present work relies on the ensemble square-root Kalman filter formulation of Whitaker and Hamill (2002). Each 6-hours the ensemble analysis updates the ensemble mean and its members through the sequence

$$\bar{\mathbf{w}}^a = \bar{\mathbf{w}}^b + \sum_{j=1}^{p} \mathbf{k}_j \left[y_j - h_j(\bar{\mathbf{w}}^b) \right] \tag{3a}$$

$$\Delta\mathbf{w}_m^a = \Delta\mathbf{w}_m^b - \sum_{j=1}^{p} \mathbf{k}_j \gamma_j \delta h_{m;j} \, , \tag{3b}$$

where y_j is the j-th observation, $\delta h_{m;j}$ is the j-th element of the incremental factor $\delta\mathbf{h}_m \equiv \mathbf{H}\Delta\mathbf{w}_m \approx \mathbf{h}(\mathbf{w}_m^b) - \mathbf{h}(\bar{\mathbf{w}}^b)$ resulting from the fact that observations are not perturbed in this formulation, and the n_w-vector $\mathbf{k}_j$ is the j-th column of the gain matrix, $\mathbf{K}$, and is given by

$$\mathbf{k}_j = \frac{1}{M-1} \sum_{m=1}^{M} \Delta\mathbf{w}_m^{j-1} \delta h_{m;j} / \sigma_j^2 \tag{4a}$$

$$\Delta\mathbf{w}_m^j = \Delta\mathbf{w}_m^{j-1} - \mathbf{k}_j \gamma_j \delta h_{m;j} \tag{4b}$$

for $j = 1, , 2 \ldots , p$, $\Delta\mathbf{w}_m^0 \equiv \Delta\mathbf{w}_m^b$, and scalar coefficients σ_j^2 and γ_j given by

$$\sigma_j^2 \equiv \frac{1}{M-1} \sum_{m=1}^{M} (\delta h_{m;j})^2 + (\sigma_j^o)^2 \, , \tag{5}$$

$$\gamma_j \equiv 1 / \left[\sqrt{M-1} (1 + \sigma_j^o / \sigma_j) \right] \, , \tag{6}$$

Here only the diagonal elements $(\sigma^o)_j^2 \equiv (\mathbf{R})_{jj}$ of the observation error covariance are referred to, given that observation errors are assumed to be uncorrelated thus allowing observations to be processed serially (e.g., Houtekamer and Mitchell 2001); the algorithm above is a direct application of the expressions in Appendix II.E of Bierman (1977) for when the square-root of the background error covariance is made up of column vectors $\Delta\mathbf{w}_m^b$, for $m = 1, 2, \ldots , M$. After all p observations are processed, $\Delta\mathbf{w}_m^p = \Delta\mathbf{w}_m^a$, which is obtained by a backward recursion of (4b) from $j = p$ to $j = 1$ to obtain (3b). Just as when solving the variational hybrid problem, localization is also needed and used in the square-root Kalman filter formulation of Whitaker and Hamill (2002), though it is left out of the equations above for the sake of notational simplicity.

The final ensemble of analyses, ultimately used to serve as initial conditions for the ensemble of forecasts, are typically re-centered around the variational analysis and inflated by scaled perturbations $\boldsymbol{\epsilon}_m$. That is, the m-th member final analysis is given by

$$\mathbf{w}_m^a := \mathbf{w}_m^a - \bar{\mathbf{w}}^a + \mathbf{T}\mathbf{x}^a + \mu\boldsymbol{\epsilon}_m \, , \tag{7}$$

where the parameter μ specifies the magnitude of the additive perturbation, and ideally, the operator $\mathbf{T}$ converting the high-resolution variational analysis onto the n_w-dimensional space of the ensemble satisfies the relation $\mathbf{T}\mathbf{T}^T = \mathbf{I}_{n_w}$, though presently in our implementation this is not the case. Note that, in the application to GEOS ADAS, the operator $\mathbf{T}$ involves remapping of the central analysis to the topography of each member. Re-centering prevents the ensemble from steering far from the (hybrid) variational analyses, and additive inflation is one way of boosting error growth (e.g., Mitchell et al. 2002, Houtekamer et al. 2005, and Hamill and Whitaker 2005).

The *second* hybrid strategy examined in the present work relies on the “filter-free” procedure, constructed by simply replacing expression (7) with

$$\mathbf{w}_m^a = \mathbf{T}\mathbf{x}^a + \alpha\boldsymbol{\epsilon}_m \, , \tag{8}$$

completely removing the EnKF component from the cycle. By construction, the mean ensemble analysis equals the variational (hybrid) analysis, aside from differences in resolution. Notice that both strategies (7) and (8) employ the same additive perturbation $\boldsymbol{\epsilon}_m$, which in practice means pooling from the same database on 48-minus-24-hour forecast NMC-method-like differences.

3. GEOS ADAS 3DVar Ensemble Hybrid

In GOES ADAS the variational problem of minimizing (1) is solved using the Grid-point Statistical Interpolation (GSI; Kleist et al. 2009a) analysis and the preconditioning formulation of (Derber and Rosati 1989). The static background error covariance matrix is implemented as a series of recursive filters producing nearly Gaussian and isotropic correlation functions following Wu et al. (2002), and tuned from GEOS forecasts (Wei Gu contribution in Rienecker et al. 2008); the hybrid background error covariance matrix uses an ensemble of GEOS background fields in a hybrid-capable GSI (David F. Parrish, personal communication). Satellite radiances are processed using the Community Radiative Transfer Model (CRTM; Kleespies et al. 2004) and the online variational bias-correction procedure of Derber and Wu (1998). A normal-mode-based balance constraint term following Kleist et al. (2009b) is applied to the static increment as well as to the ensemble part of the increment whenever the hybrid analysis is used.

The ensemble hybrid-capable GEOS ADAS relies on the GEOS global atmospheric general circulation model (AGCM), developed at NASA/Goddard. The GEOS AGCM is built under the infrastructure of the Earth System Modeling Framework (ESMF; Collins et al. 2005) and couples a cubed-sphere hydrodynamics (Putman and Lin 2007) with various physics packages including a modified version of the Relaxed Arakawa-Schubert convective parameterization scheme of Moorthi and Suarez (1992), the catchment-based hydrological model of Koster et al. (2000), the multi-layer snow model of Stieglitz et al. (2001), and the radiative transfer model of Chou and Suarez (1999), which uses interactive climatological aerosols from the Goddard Global Ozone Chemistry Aerosol Radiation and Transport

(GOCART; Collarco et al. 2010) package.

In GEOS ADAS, assimilation is performed using the incremental analysis update (IAU) procedure of Bloom et al. (1996). A schematic representation of standard IAU appears in the top panel of Fig. 2. Considering for example the availability of observations around 00 UTC and of three-hourly AGCM background fields, the GSI analysis (purple boxes) produces an increment that is converted into a tendency and used to force a 6-hour (corrector) model integration (red triangles); this is followed by a 6-hour (predictor) integration period when the model is then set to run free from the analysis forcing as to produce backgrounds (green, upside-down, triangles) for the next assimilation cycle; the prediction period can be extended beyond 6-hours to complete, say, a 5-day forecast (horizontal orange-dashed lines). The cycle of running GSI and AGCM takes place whether GEOS ADAS is performing its traditional 3DVar procedure or its hybrid extension. The only difference between these two options is that in the latter case, an ensemble of background fields is required for GSI to internally augment its background error covariance information, through (1). Hereafter, this cycle will be referred to as the *central* ADAS. It usually operates at a higher resolution than the ensemble ADAS (see below).

Generation of the ensemble of background fields to make up the ensemble background error covariance $\mathbf{B}_e$ involves AGCM integrations similar to those of the central ADAS, but generally carried at lower resolution. In turn, the ensemble of backgrounds requires an ensemble of "initial conditions" (analyses) to be available. At least three options exist within GEOS ADAS to generate an ensemble of analyses. The standard option follows Whitaker et al. (2008), as described earlier, and relies on the ensemble Kalman filter (EnKF) software of

J. S. Whitaker, from NOAA/ESRL. This is the same software presently used in the NCEP operational global data assimilation system. Alternatively, one can generate an ensemble of GSI analyses, but this is considerably more computationally demanding than using the EnKF since it involves a complete variational analysis for each member of the ensemble. And lastly, an option to exercise the filter-free ensemble analysis is also available. Regardless of the ensemble of analyses scheme, once analyses are available, a corresponding set of background fields is generated through IAU-based AGCM integrations, similar to those of the central ADAS. The IAU-based ensemble procedure is illustrated in the bottom panel of Fig. 2. Availability of observations and an ensemble of backgrounds triggers one of the ensemble analysis options (EnAna; right-placed, purple boxes), including re-centering and additive inflation, generating an ensemble of analyses which are then turned into an ensemble of tendencies used to initialize the ensemble of AGCM integrations — forced during the first 6 hours (light-red triangles), and unforced during the 6-hour background prediction period (light-green, upside-down triangles).

There is a subtle difference to note related to how the GEOS ADAS IAU-based ensemble evolves its members when the EnKF is used versus when the filter-free strategy is used instead. With the EnKF, each member permanently cycles its corresponding set of initial conditions needed by the GEOS AGCM each cycle. With the filter-free strategy, the initial conditions for the ensemble of AGCM integrations are generated by simply converting the (high-resolution) initial conditions from the central (hybrid) cycle to the configuration of the ensemble; namely, at each cycle, all members start from the exact same set of initial conditions; the only thing making these integrations distinct is the corresponding IAU forcing term used by each member, each derived from the ensemble analysis equation (8).

4. Evaluation of hybrid strategies in GEOS ADAS

In what follows, we present a discussion of results obtained for experiments from single analysis as well as fully cycled ADAS. Regular, non-hybrid, 3DVar results are compared with results from hybrid 3DVar analyses produced at 0.5-degree resolution on 72 vertical levels and relying on a 32-member, 1-degree, 72-level ensemble generated by either the EnKF or the filter-free procedure described above.

a. Non-cycling hybrid analysis

When an ensemble of backgrounds is used in a hybrid GSI analysis, one of the first things we examined was how the analysis increment changed with respect to its non-hybrid counterpart. Figure 3 provides an illustration for the change in analysis increment, measured in total energy units, for an analysis calculated at a single synoptic time using: (i) regular 3DVar, with only the static background error covariance (left); (ii) 3DVar with a background error covariance matrix that is fully determined by the 32-member ensemble (center); and (iii) 3DVar hybrid, when 50% of background error covariance matrix comes from the ensemble and the remaining 50% comes from its regular static background error covariance matrix (right). The ensemble-only case (center) shows considerably more activity in the tropics than when compared with the static-only case (left); the resulting hybrid (right) increment shows slight, but noticeable, energy increase in the mid-tropospheric and low-stratospheric levels — a little less energy seems to be present along the Southern tropospheric jet in the ensemble (center) when compared to the static case (left), with the resulting hybrid retaining the energy in this region (right).

Another aspect of relevance when introducing upgrading to hybrid analyses relates to how balance gets affected. In its 3DVar configuration, GSI has the capability of applying a tangent linear normal mode constraint (TLNMC) to the increment (see Kleist et al. 2009b). The constraint can be applied to either part of the increment (essentially to either of the two terms in eq. 2, or both; see Kleist 2012). Figure 4 shows two illustrations of the result of balancing the increment in various configurations of GSI. The panel on the left shows the total cost function during the iterations of the GSI minimization when using: traditional 3DVar without TLNMC (black curve); traditional 3DVar with TLNMC (red curve); hybrid 3DVar with TLNMC applied only to the static part of increment (green); and hybrid 3DVar when TLNMC is applied to the full increment. The behavior is typical of when adding constraints to the analysis, that is, with balance, the cost settles a little higher than when no constraint is applied. The hybrid minimization tends to reduce the cost when compared to the static-balanced configuration; particularly noticeable in the first outer minimization (first 100 iterations; compare green and blue curves with red curve, respectively). This is indication that the hybrid minimization recovers the fit to the observations somewhat deteriorated when the constraint is added to traditional 3DVar.

The real measure of improved balance is displayed in the right panel of Fig. 4 where the spectra of the vertically integrated mass-wind divergence increment is shown for the same four configurations. The color scheme is preserved, and the curves show clearly that

TLNMC brings in considerable improvement in balance when applied to traditional 3DVar (compare black and red curves). It is also clear from the figure that applying TLNMC only to the static part of the increment when hybrid 3DVar is used is rather troublesome (green curve). This is natural since nothing guarantees the ensemble contribution to the increment, through its background error covariance matrix $\mathbf{B}_e$, to be balanced in any way; TLNMC must be applied to the full increment (blue curve) for balance to be acceptable in the hybrid configuration. However, this latter case is not completely perfect since some power in the spectrum still remains for large wave numbers which would best be reduced. As pointed out by Kleist (2012; see Figure 4.2 on page 108, in that work), this is a consequence of the dual-resolution aspect of the hybrid analysis and some aliasing of the winds. It is possible to use scale-dependent weights to reduce some of the aliasing issue (see Kleist 2012, Fig. 4.4, in that work), but this is part of future work. At present, the default in GEOS hybrid ADAS is to apply TLNMC to the full increment.

The remaining illustrations in this section summarize results and comparisons from three experiments covering the month of April 2012. The abbreviations and brief explanation of each experiment follows:

- Control (CTL): traditional 3DVar, similar to what is used by GMAO Operations, though experiments here are at, coarser, 0.5-degree resolution.

- Hybrid (HY5): Dual-resolution hybrid ADAS using 50% static and 50% ensemble background error covariance contributions, with an ensemble of analyses generated by the EnKF.

- Hybrid (HYA): similar to HY5, but using the filter-free procedure, that is, at each cycle, an ensemble of analyses is generated by adding scaled NMC-like perturbations to the hybrid (central) variational analysis.

Evaluation of results of these experiments examine familiar diagnostics: observation-minus-analysis (OMA), observation-minus-background (OMB), and observation-minus-forecast (OMF) residual statistics, monthly mean comparison with corresponding means from other numerical weather prediction (NWP) centers, and forecast skills scores. Additionally, ensemble-related diagnostics have also been examined to evaluate the performance of the ensemble itself. These included monthly-mean of the ensemble mean analyses and/or backgrounds, OMA, OMB and OMF residual statistics for the mean and ensemble members, and also time evolution of ensemble spread. Rank histograms (of say, OMB residuals) have been looked but we have found them to be rather difficult to interpret given the uncertainties associated with the observations (see Hamill 2001), therefore we refrain from discussing them here.

b. About the ensemble itself

We have seen in Fig. 1 how much re-centering and additive inflation participate to modify the analysis increments calculated by the EnKF. In addition to what was said earlier, we should point out that we have found re-centering and additive inflation to be necessary within the context of the small-size ensemble GEOS hybrid ADAS. Without re-centering the EnKF analyses were found to diverge from the central hybrid analysis; without additive inflation the ensemble was found to collapse rather quickly. Furthermore, finding the scaling parameter α multiplying the additive inflation term requires careful tuning. We have found a value of 0.25 to be rather reasonable when the EnKF is used. This is considerably lower than value of 0.40 presently used in the NCEP hybrid 3DVar (Daryl Kleist, pers. comm.). However, when using the filter-free approach, the value of 0.40 was found to be more adequate.

In a cycling situation, the interplay between re-centering and inflation must lead to reasonable forecast spread. Figure 5 illustrates the time evolution of the global (largely tropospheric) spread of a 32-member ensemble for typical experiments performed with GEOS hybrid ADAS. The panel on the left uses the EnKF for its ensemble analysis and shows how the initial spread (blue curve) changes as the members evolve within the 9-hour background period (green, red, and black for the 3-, 6- and 9-hour backgrounds, respectively). The resulting hybrid ADAS performs rather well (see below), even when there is not much error growth within the 9-hour background period — note the green, red and black curves are very close to each other; however, the growth of error is consistent within the same period, with the smallest error seen in the 3-hr background and the largest in the 9-hour background. The panel on the right shows similar forecast spread for various times within the background period, but now when the filter-free approach is used to generate the ensemble of analyses. The initial spread is zero by construction (blue curve); the overall error growth is smaller than when the EnKF is used, and the error growth for within the 6-hour background period is now considerably larger. However, as we will see shortly, even with this difference in forecast spread within the 6-hour background period, the end result between the two ensemble generation procedures is very similar to the corresponding hybrid ADAS performing rather closely.

c. *Evaluation with respect to observations*

Figure 6 shows vertical profiles of *monthly averaged* zonal wind (top) and temperature (bottom) radiosonde OMB residuals over three regions of the globe, namely, Northern Hemisphere (NH; left), tropics (center), and Southern Hemisphere (SH; right). Two hybrid experiments, one using the EnKF (HY5, red) and another using the filter-free scheme (HYA, green), are compared to the traditional 3DVar control experiment (CTL, blue). The only noticeable differences are in the tropics and SH for zonal winds, where the hybrid experiments show reduced biases with respect to the control; the EnKF and simplified (filter-free) scheme are rather comparable to each other. Results for temperature remain rather neutral. Examination of *standard deviation* of the OMB residuals for both winds and temperature indicate negligible differences among all three experiments (not shown).

It is also possible to examine the impact of observations on the analysis following Todling (2013). This is an observation-space approach that uses the inverse of the observation error variances to define a measure for evaluating the contribution of various observing systems to the cycling assimilation. Fig. 7 displays impact results for the three experiments under consideration: control (black), EnKF-based hybrid (cyan), and filter-free-based hybrid (magenta). Regardless of the underlying analysis procedure, all three experiments show aircraft, radiosondes, and Aqua AIRS as the dominating observing systems in GEOS ADAS. These observing systems tend to display smaller impact when the cycling analysis is based on a hybrid approach as compared to traditional 3DVar — the hybrid strategies seem to rely slightly more on these observing systems than does traditional 3DVar.

Figure 8 shows vertical profiles of standard deviations, calculated over the month of April

2012, for zonal wind radiosonde OMF residuals of the 24 hour forecasts. Though rather small, the benefit of using a hybrid assimilation strategy shows in both the tropics and Southern Hemisphere. Again here, the difference between the EnKF-based system and that using the filter-free configuration is very small, with some advantage shown for the latter in the SH.

d. Evaluation with respect to independent analysis

We routinely compare monthly mean analyses with those from other NWP centers. Figure 9 shows the differences of the April 2012 zonally-averaged zonal wind for each experiment with the corresponding ECMWF operational analysis. Panels in the figure are differences for the control (CTL, top left), the filter-free hybrid scheme (HYA, top right), and the EnKF-based hybrid (HY5, bottom left). Compared with the control, both hybrid procedures obtains monthly mean analysis considerably closer to ECMWF's monthly mean analysis; this is especially noticeable in the tropics. The bottom-right panel shows the monthly mean of the ensemble mean EnKF analysis (from HY5) difference with ECMWF operational analysis. Comparing this result with, say, that in the bottom-left panel, illustrates the behavior and reliability of the underlying EnKF ensemble analyses, though in the presence of re-centering it serves mainly as a sanity check to show that inflation averages away.

e. Evaluation with respect to self analysis

Lastly, we show some results when comparing forecasts from each of the three experiments with their own respective analyses. Figure 10 displays the zonally-averaged wind RMS error of the 24 hour forecast, as a function of pressure, for three regions of interest. Results are for the three experiments under consideration: control (blue), and the two EnKF (HY5, red) and filter-free (HYA, green) hybrid strategies. Both hybrid strategies yield the same improvement in RMS error in the Northern and Southern Hemispheres, but result in some deterioration in Tropical mid-troposphere, with the filter-free procedure being less damaging than the EnKF. This behavior is opposite to that seen when examining both the monthly mean analyses and mean OMB radiosonde residuals, in which hybrid strategies amounted to improvement over traditional 3DVar. This remains an issue to tackle in future studies with GEOS Hybrid ADAS.

In many ways, successful procedures must amount to improvement in the 500 hPa geopotential height anomaly correlations. Self-analysis evaluation results appear in Fig. 11 for 5-day forecasts in both Northern (top-right) and Southern Hemisphere (top-left). Curves for the control experiment are in blue, those for the EnKF-based hybrid are in red, and those for the filter-free strategy are in green. The corresponding statistical significance curves appear at the bottom panels. The NH scores are pretty much neutral, but those in the SH show significant benefit from hybrid assimilation (bottom-left shows red and green curves outside and above significance boxes). Both hybrid strategies bring comparable and non-negligible improvements up to 5 days in their forecasts. We must stress the word comparable, as we see the filter-free procedure amounting to rather indistinguishable performance from a system using the EnKF to generate the ensemble of analyses.

5. Closing remarks

In the process of implementing a 3DVar hybrid strategy for the Goddard Earth Observing System (GEOS) atmospheric data assimilation system (ADAS) using the ensemble Kalman filter (EnKF) of Whitaker and Hamill (2002), under a dual resolution approach, we have found re-centering and additive inflation to play a fundamental role in determining the behavior of the ensemble. Examination of some preliminary results led us to consider generating the ensemble by simply adding NMC-method-like perturbations to the central (hybrid) variational analysis at each cycle, thus completely bypassing the EnKF. This so-called filter-free procedure was put to the same evaluation test suite as that used to examine the quality of our EnKF-based 3DVar hybrid implementation. Both schemes are shown to perform rather similarly, bringing statistically significant improvements to GEOS ADAS. Indeed, the improvements to GEOS ADAS due to hybridization are comparable in magnitude to those seen at NCEP when upgrading its 3DVar system to a hybrid strategy, around May 2012. The successful evaluation of the filter-free approach is encouraging since one of its main advantages relates to not having to maintain two considerably different analysis systems, namely, one to perform the EnKF and another to perform the 3DVar hybrid analysis (the Grid-point Statistical Interpolation analysis, in the present case). Though not the main driving motivation for this work, it is also important to stress the computational advantages of the filter-free approach over the EnKF, or any alternative ensemble filter scheme, since the filter-free scheme does not explicitly analyze the members of the ensemble.

At this point, we can only attempt to speculate on the reasons why the EnKF and filter-free procedures perform so similarly. Factors that are likely to contribute to this are the small size of the ensemble, and the dual resolution aspect of the GEOS ADAS implementation. Future tests are planned to accurately evaluate the role solely due to the resolution interplay. Further tests are also planned to look at the role played by the size of the ensemble, though we expect these to be harder to accurately provide conclusive results since they may require too large an ensemble to possibly afford in real applications such as the ones presented here.

Acknowledgments.

The authors are thankful to David F. Parrish, Darly Kleist, Russ Treadon, and John Derber, from NOAA/NCEP, for the multiple discussions during the period of implementation of the hybrid components of the GEOS ADAS, particularly in what refers to GSI- and EnKF-related settings. The authors are also thankful to Jeffrey S. Whitaker, from NOAA/ESRL, for a number of discussions throughout the course of implementation of his EnKF software in our system. Results were obtained using support and computing resources from the NASA Center for Climate Simulation at Goddard Space Flight Center.

REFERENCES

Bierman, G. L., 1977: *Factorization Methods for Discrete Sequential Estimation*. Dover Publications, 241 pp.

Bloom, S. C., L. L. Takacs, A. M. da Silva, and D. Ledvina, 1996: Data assimilation using incremental analysis updates. *Mon. Wea. Rev.*, **124**, 1256–1271.

Buehner, M., P. L. Houtekamer, C. Charette, H. L. Mitchell, and B. He, 2010: Intercomparison of variational data assimilation and the ensemble kalman filter for global deterministic nwp. part ii: One-month experiments with real observations. *Mon. Wea. Rev.*, **138**, 1567–1586.

Chou, M.-D. and M. J. Suarez, 1999: A shortwave radiation parameterization for atmospheric studies. Tech. rep., NASA. TM 104606, Vol. 15, 40 pp.

Clayton, A. M., A. C. Lorenc, and D. M. Barker, 2012: Operational implementation of a hybrid ensemble/4d-var global data assimilation system at the met office. *Q. J. Royal Meteorol. Soc.*, doi:10.1002/qj.2054.

Collarco, P., A. da Silva, M. Chin, and T. Diehl, 2010: Online simulations of global aerosol distributions in the nasa geos-4 model and comparisons to satellite and ground-based aerosol optical depth. *J. Geophys. Res.*, **155**, D14 207.

Collins, N., et al., 2005: Design and implementation of components in the Earth System Modeling Framework. *Intl. J. High Perform. Comput. Appl.*, **19(3)**, 341–350.

Derber, J. C. and A. Rosati, 1989: A global oceanic data assimilation system. *J. Phys. Oceanogr.*, **19**, 1333–1347.

Derber, J. C. and W.-S. Wu, 1998: The use of TOVS could-cleared radiances in the NCEP SSI analysis system. *Mon. Wea. Rev.*, **126**, 2287–2299.

Hamill, T. M., 2001: Interpretation of rank histograms for verifying ensemble forecasts. *Mon. Wea. Rev.*, **129**, 550–560.

Hamill, T. M. and C. Snyder, 2000: A hybrid ensemble kalman filter-3d variational analysis scheme. *Mon. Wea. Rev.*, **128**, 2905–2919.

Hamill, T. M. and J. S. Whitaker, 2005: Accounting for the error due to unresolved scales in ensemble data assimilation: A comparison of different approaches. *Mon. Wea. Rev.*, **133**, 3132–3147.

Houtekamer, P. L. and H. L. Mitchell, 2001: A sequential ensemble kalman filter for atmospheric data assimilation. *Mon. Wea. Rev.*, **129**, 123137.

Houtekamer, P. L., H. L. Mitchell, G. Pellerin, M. Buehner, M. Charron, L. Spacek, and B. Hansen, 2005: Atmospheric data assimilation with an ensemble kalman filter: Results with real observations. *Mon. Wea. Rev.*, **133**, 604620.

Kleespies, T. J., P. van Delst, L. M. McMillin, and J. Derber, 2004: Atmospheric transmittance of an absorbing gas. 6. OPTRAN status report and introduction to the NESDIS/NCEP Community Radiative Transfer Model. *Appl. Opt.*, **43**, 3103–3109.

Kleist, D. T., 2012: An evaluation of hybrid variational-ensemble data assimilation for the NCEP GFS. Tech. rep., Univ. of Maryland. Ph.D. Thesis, 163 pp. [Available at http://www.emc.ncep.noaa.gov/gmb/wd20dk/docs/phd/DarylKleist_PhDThesis_Revised.pdf].

Kleist, D. T., D. F. Parrish, J. C. Derber, R. Treadon, R. M. Errico, and R. Yang, 2009b: Improving incremental balance in the GSI 3DVAR analysis system. *Mon. Wea. Rev.*, **137**, 1046–1060.

Kleist, D. T., D. F. Parrish, J. C. Derber, R. Treadon, W.-S. Wu, and S. Lord, 2009a: Introduction of the GSI into the NCEPs Global Data Assimilation System. *Wea. Forecasting*, **24**, 1691–1705.

Lorenc, A. C., 2003: The potential of the ensemble Kalman filter for NWP–A comparison with 4D-Var. *Q. J. Royal Meteorol. Soc.*, **129**, 3183–3203.

Mitchell, H. L., P. L. Houtekamer, and G. Pellerin, 2002: Ensemble, balance, and model-error representation in an ensemble Kalman filter. *Mon. Wea. Rev.*, **130**, 2791–2808.

Moorthi, S. and M. Suarez, 1992: Relaxed Arakawa-Schubert: A parameterization of moist convection for general-circulation models. *Mon. Wea. Rev.*, **120**, 978–1002.

Putman, W. M. and S.-J. Lin, 2007: Finite-volume transport on various cubed-sphere grids. *J. Comp. Phys.*, **227**, 55–78.

Rienecker, M. M., et al., 2008: The GEOS-5 Data Assimilation System - Documentation of Versions 5.0.1, 5.1.0, and 5.2.0. Tech. rep., NASA. TM 104606, Technical Report Series on Global Modeling and Data Assimilation, Vol. 27, 118 pp.

Stieglitz, M., A. Ducharne, R. Koster, and M. Suarez, 2001: The impact of detailed snow physics on the simulation of snow cover and subsurface thermodynamics at continental scales. *J. Hydromet.*, **2**, 228–242.

Todling, R., 2013: Comparing two approaches for assessing observation impact. *Mon. Wea. Rev.*, **141**, 1484–1505.

Wang, X., C. Snyder, and T. M. Hamill, 2007: On the theoretical equivalence of differently proposed ensemble/3d-var hybrid analysis schemes. *Mon. Wea. Rev.*, **135**, 222–227.

Whitaker, J. S. and T. M. Hamill, 2002: Ensemble data assimilation without perturbed observations. *Mon. Wea. Rev.*, **130**, 1913–1924.

Whitaker, J. S., T. M. Hamill, X. Wei, Y. Song, and Z. Toth, 2008: Ensemble data assimilation with the ncep global forecast system. *Mon. Wea. Rev.*, **136**, 463–482.

Wu, W.-S., R. J. Purser, and D. F. Parrish, 2002: Three-dimensional variational analysis with spacially inhomogeneous covariances. *Mon. Wea. Rev.*, **130**, 2905–2916.

List of Figures

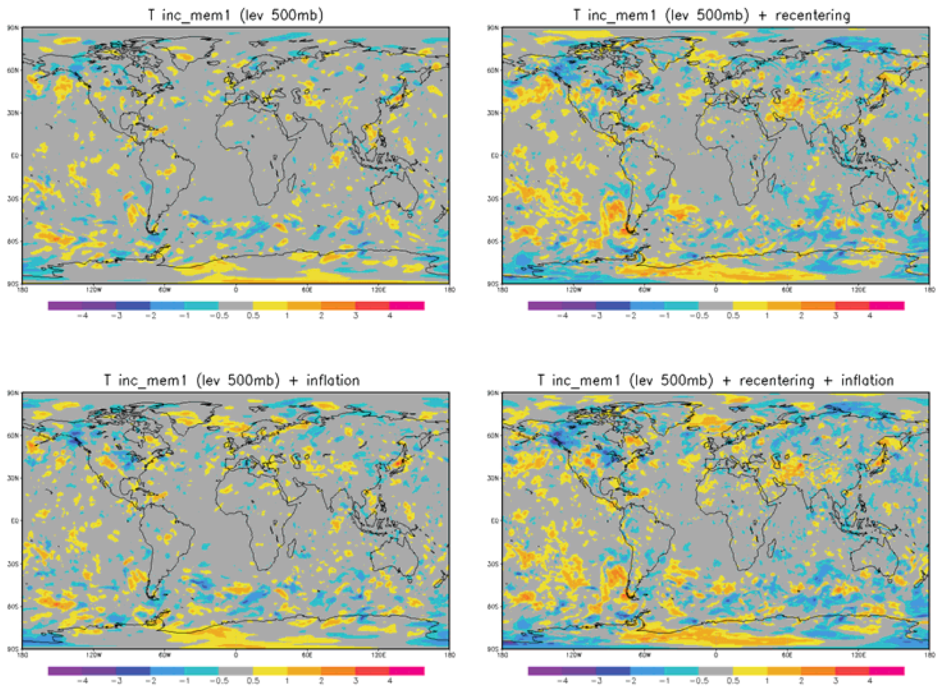

Fig. 1. Illustration of contribution from each step taking place after the EnKF ensemble of analyses are generated. The panels show 500 hPa temperature: analysis increment for a given ensemble member (top left); effect of re-centering this given member about the central GSI analysis (top right); effect of applying additive inflation to the member analysis with a coefficient of 0.25 (bottom left); and resulting increment after both re-centering and additive inflation are applied (bottom right).

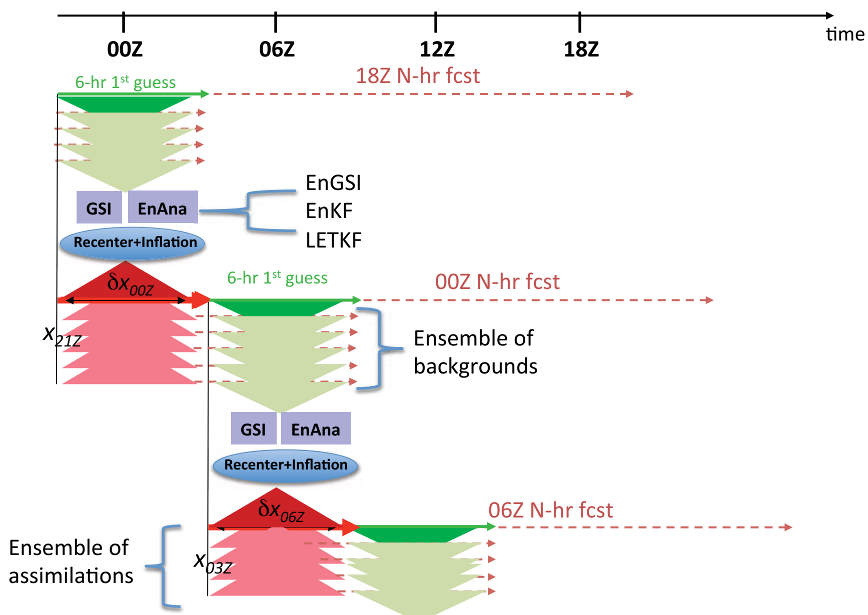

FIG. 2. Schematic of AU as implemented in GEOS hybrid ensemble-variational atmospheric data assimilation system.

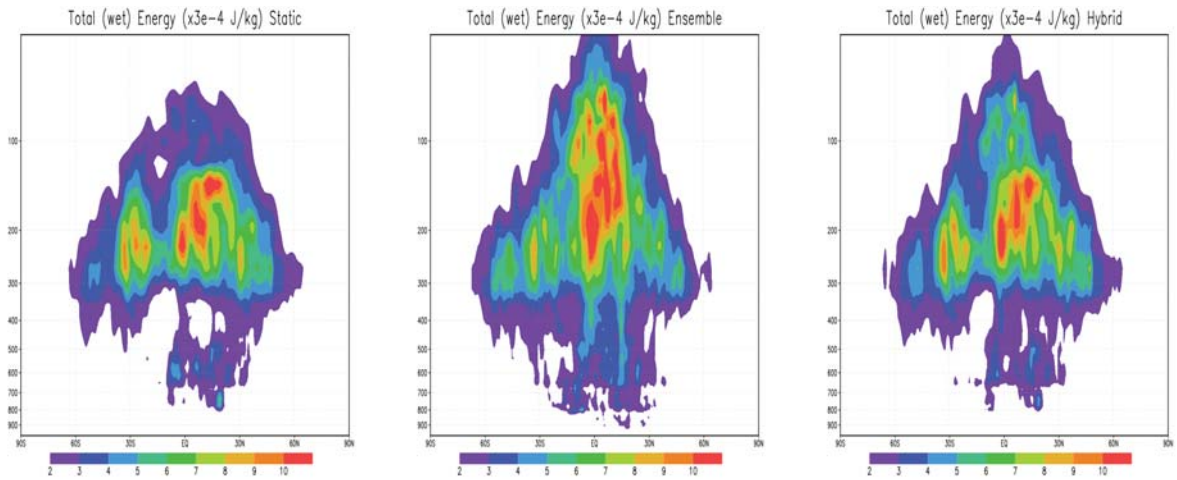

Fig. 3. Zonal mean analysis increment, in total wet energy (J/kg) norm, using a standard 3DVar (left), a 3DVar when the background error covariances are fully determined by the ensemble (center), and a hybrid 3DVar when the covariances are a 50% weighted sum of the static- and ensemble-derived background error covariances (right).

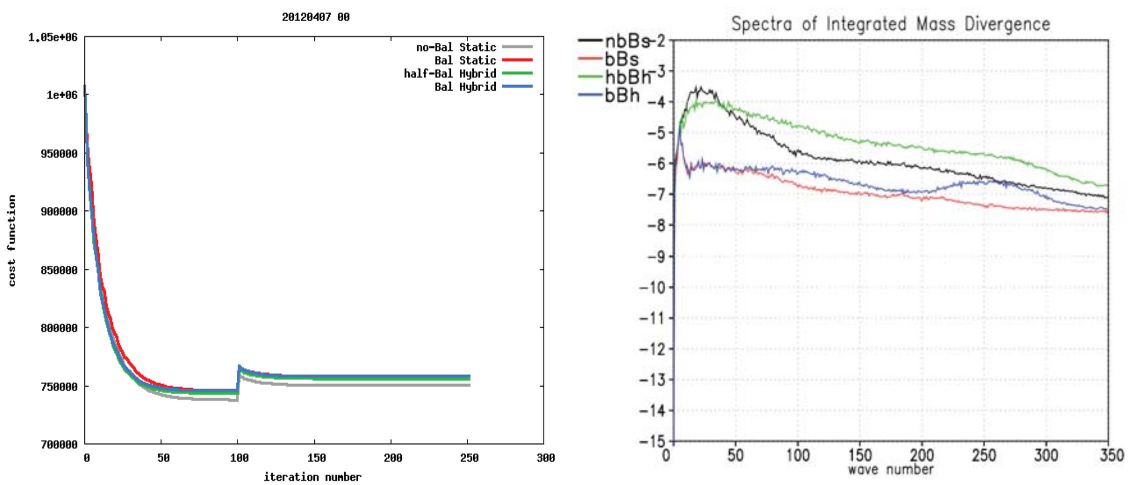

Fig. 4. The panel on the left shows the total cost function as it changes during the iterations of the GSI minimization; all cases are calculated for the same synoptic time but GSI is configured as follows: static (non-hybrid) 3DVar without balance constraint (black curve); (non-hybrid) 3DVar with TLNMC balance constraint (red curve); hybrid 3DVar without balance constraint applied to hybrid part of increment (green curve); and hybrid 3DVar with balance constraint applied to full increment (blue curve). The panel on the right shows the integrated mass-wind divergence spectra of the analysis increment as a function of wave number for the same four configurations; color scheme of curves is as in panel on the left.

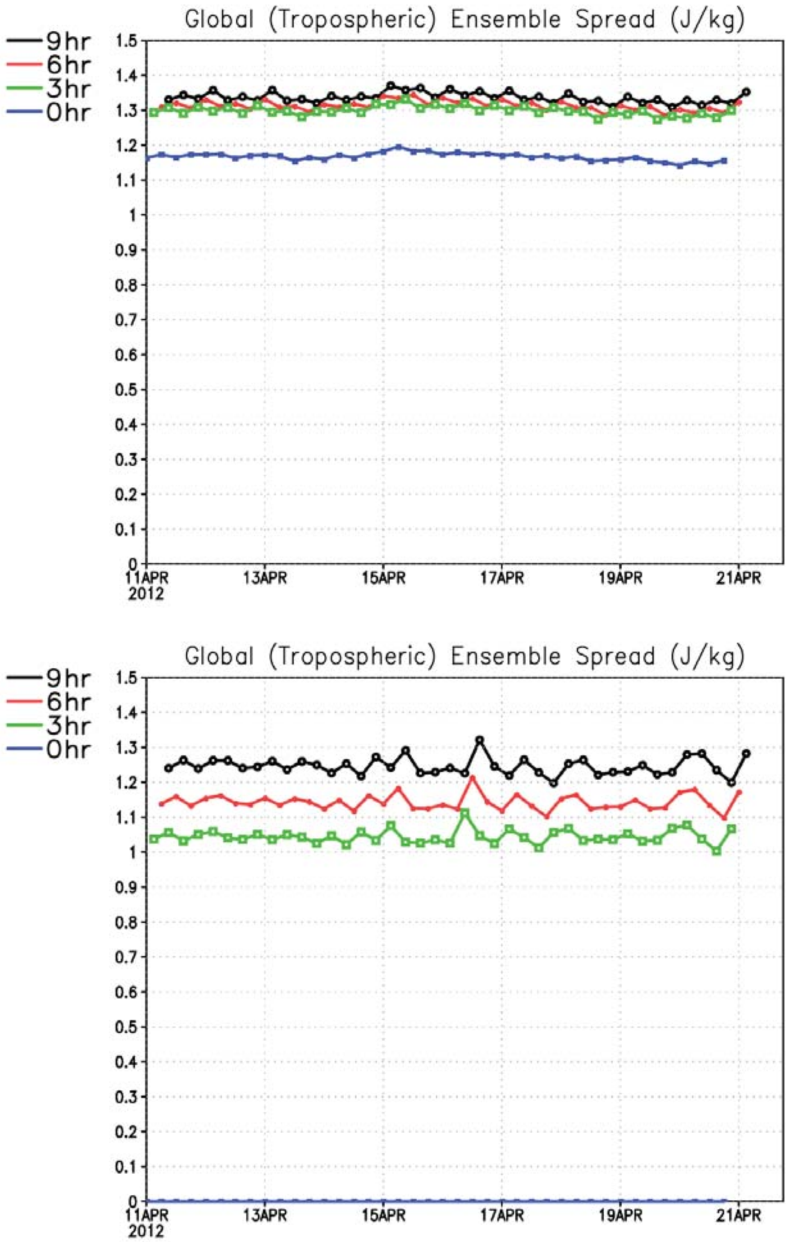

Fig. 5. Global spread of a 32-member ensemble measured in total energy units (J/kg); when EnKF is used to generate ensemble (top), and when filter-free ensemble scheme is used instead (bottom). The curves are for: analysis spread before re-centering and inflation (blue); 3-, 6- and 9-hour backgrounds (green, red, and black respectively). Totals exclude levels roughly above 10 hPa.

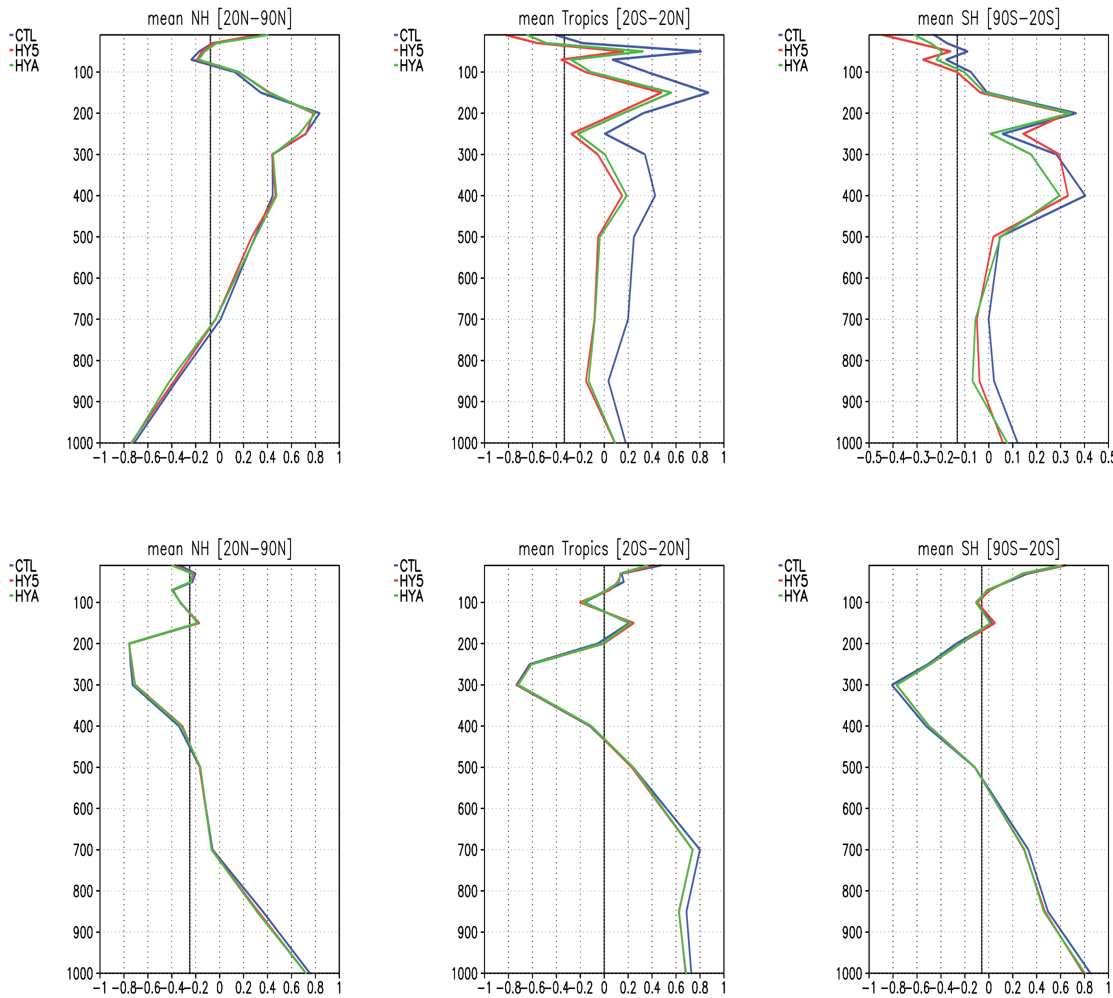

FIG. 6. Regionally-averaged, monthly mean of radiosonde OMB residuals of zonal wind (top) and temperature (bottom) for three experiments: control (blue), EnKF-based hybrid (red), and filter-free hybrid (green), shown for: Northern Hemisphere (left column), tropics (center column), and Southern Hemisphere (right column).

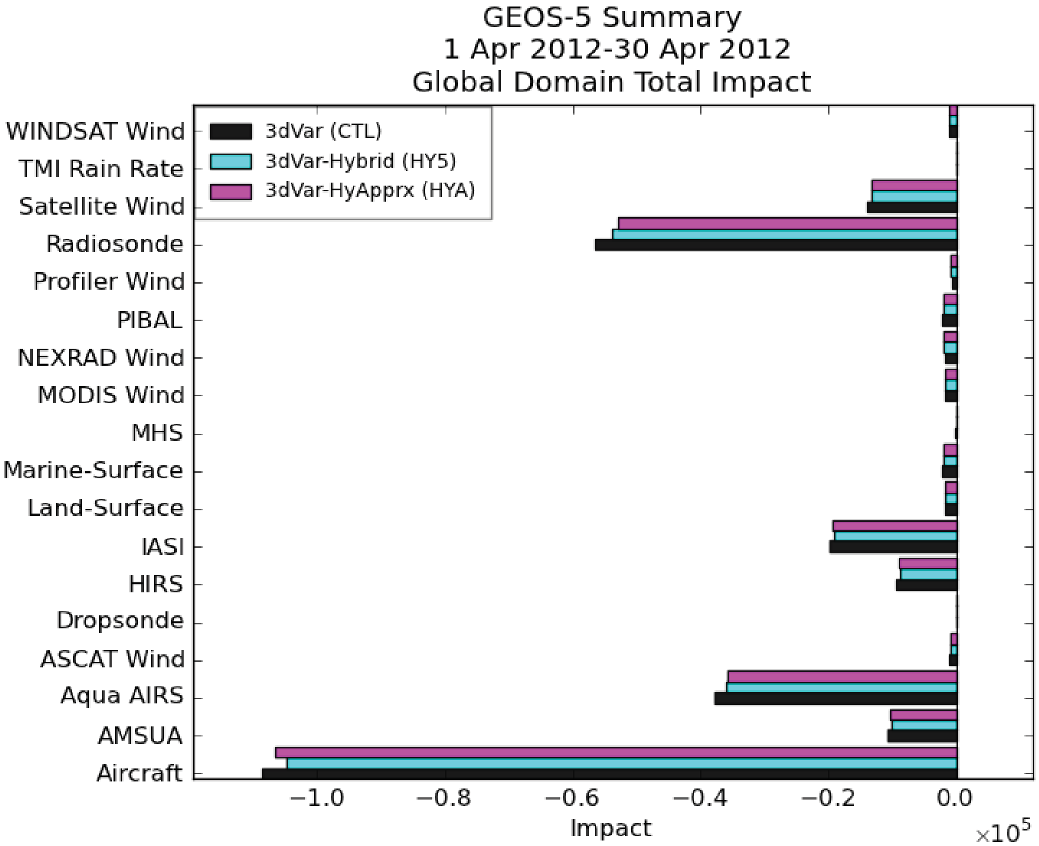

FIG. 7. Observation impact on the analysis for three 3DVar experiments: control, non-hybrid (black bars); hybrid using EnKF (cyan bars); and hybrid using simplified, filter-free approach (magenta bars). In addition to the observation types shown, all experiments use GPS radio occultation, but results are not shown here due to a little glitch in the output files saving their corresponding information (basically, GPS impacts are of the magnitude of those of radiosondes, and are comparable among the difference analysis approaches).

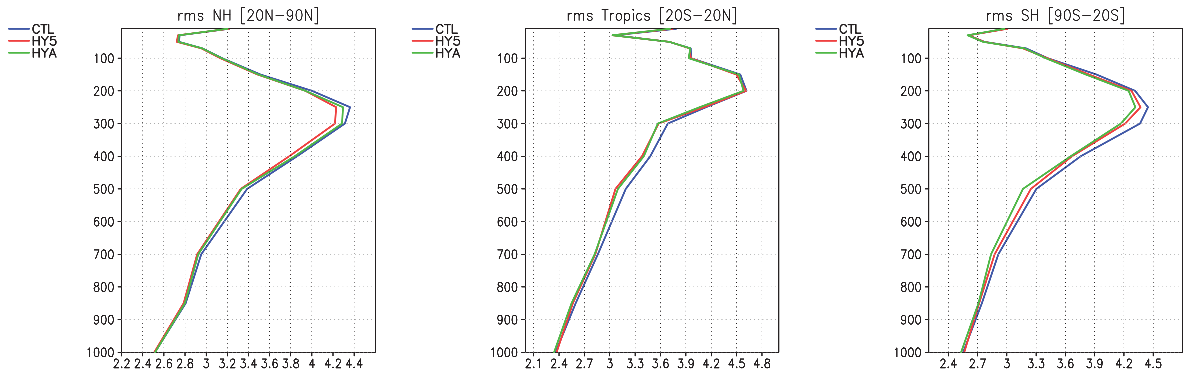

FIG. 8. Similar to Fig. 6, but for standard deviation. Only zonal winds are shown since temperature have neutral results.

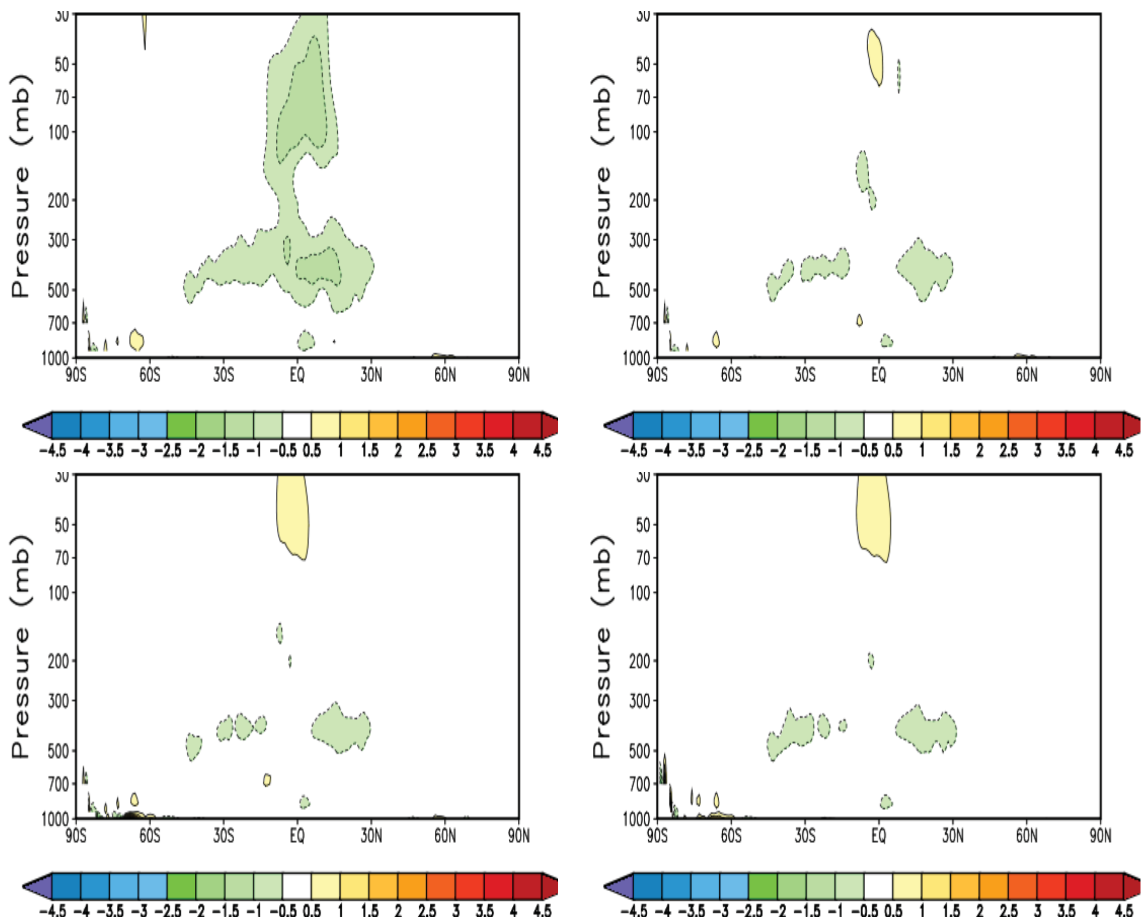

Fig. 9. April 2012 monthly mean of zonally-averaged zonal wind analysis differences with ECMWF operational analysis from four different ADAS scenarios: control, traditional 3DVar (top left); filter-free-based hybrid 3Dvar (top right); EnKF-based hybrid 3DVar (bottom left); and EnKF ensemble mean (bottom right).

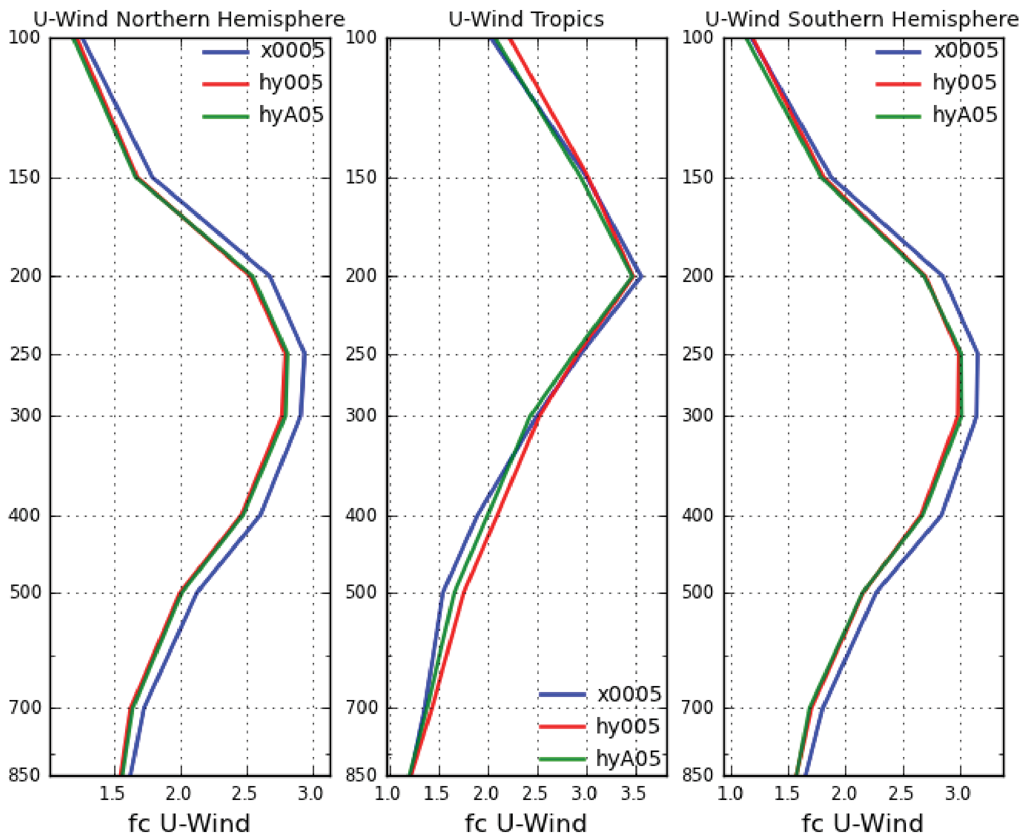

Fig. 10. Twenty-four hour forecast RMS error, with respect to self-analysis, of regionally-averaged zonal winds for the three experiments under consideration: control (blue), EnKF-based hybrid (red), and filter-free hybrid (green); Northern Hemisphere (left), tropics (center), and Southern Hemisphere (right).

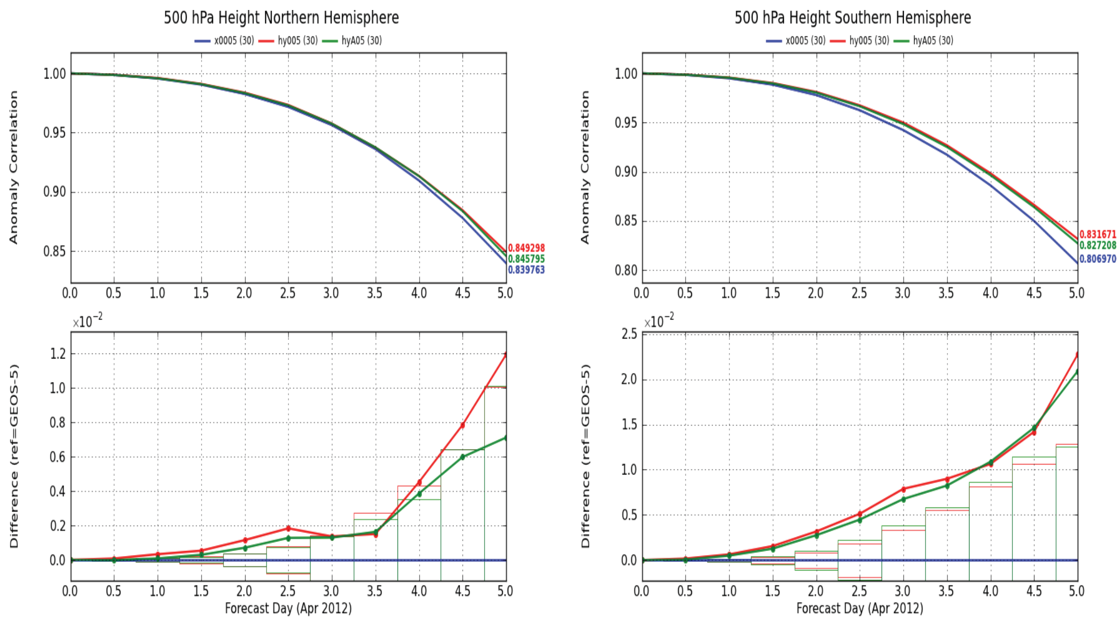

Fig. 11. Anomaly correlation of the 500 hPa height of 5-day forecasts (top) verified with respect to own analysis, and shown for Northern (left) and Southern (right) Hemispheres for the three experiments under consideration: the control (blue), EnKF-based hybrid (red), and filter-free hybrid (green). Significance plots appear beneath anomaly correlations with significance boxes color according to experiment designation; results are statistically significant when curve appear outside, and above, corresponding box.